

Article

Thiosemicarbazones and Derived Antimony Complexes: Synthesis, Structural Analysis, and In Vitro Evaluation against Bacterial, Fungal, and Cancer Cells

Amany Fathy¹, Ahmed B. M. Ibrahim^{2,*}, S. Abd Elkhaliq¹, Florian Meurer³, Michael Bodensteiner³
and S. M. Abbas¹

¹ Chemistry Department, Faculty of Science, Beni-Suef University, Beni-Suef 62521, Egypt

² Department of Chemistry, Faculty of Science, Assiut University, Assiut 71516, Egypt

³ Faculty of Chemistry and Pharmacy, University of Regensburg, Universitätsstraße 31, 93053 Regensburg, Germany

* Correspondence: aibrahim@aun.edu.eg

Abstract: Two antimony complexes {[Sb(L¹)Cl₂] **C1** and [Sb(L²)Cl₂] **C2**} with the thiosemicarbazone ligands {**HL**¹ = 4-(2,4-dimethylphenyl)-1-((pyridin-2-yl)methylene)thiosemicarbazide and **HL**² = 4-(2,5-dimethoxyphenyl)-1-((pyridin-2-yl)methylene)thiosemicarbazide} were introduced. The structures were elucidated on the basis of a CHNS analysis, spectroscopic techniques (UV-Vis and FT-IR), and DMF solution electrical conductivities. Single crystal X-ray diffraction analysis of complex **C1** assigned the complex pseudo-octahedral geometry and triclinic P-1 space group. Only the ligand **HL**¹ and its derived complex **C1** displayed antifungal activities against *Candida albicans* and this activity was enhanced from 10 mm to 21 mm for the respective complex, which is the same activity given by the drug “Amphotericin B”. The ligands **HL**¹ and **HL**² gave inhibitions, respectively, of 14 and 10 mm against *Staphylococcus aureus* and 15 and 10 mm against *Escherichia coli*; however, complexes **C1** and **C2** increased these inhibitions to 36 and 32 mm against *Staphylococcus aureus* and 35 and 31 mm against *Escherichia coli* exceeding the activities given by the ampicillin standard (i.e., 21 mm against *Staphylococcus aureus* and 25 mm against *Escherichia coli*). Against MCF-7 human breast cancer cells, the IC₅₀ values of **HL**¹ (68.9 μM) and **HL**² (145.4 μM) were notably enhanced to the values of 34.7 and 37.4 μM for both complexes, respectively. Further, the complexes induced less toxicity in normal BHK cells (**HL**¹ (126.6 μM), **HL**² (110.6 μM), **C1** (>210.1 μM), and **C2** (160.6 μM)). As a comparison, doxorubicin gave an IC₅₀ value of 9.66 μM against MCF-7 cells and 36.42 μM against BHK cells.

Keywords: main group element; penta-coordinate antimony; X-ray crystal structure; bacteria; fungi; cancer



Citation: Fathy, A.; Ibrahim, A.B.M.; Abd Elkhaliq, S.; Meurer, F.; Bodensteiner, M.; Abbas, S.M. Thiosemicarbazones and Derived Antimony Complexes: Synthesis, Structural Analysis, and In Vitro Evaluation against Bacterial, Fungal, and Cancer Cells. *Inorganics* **2022**, *10*, 172. <https://doi.org/10.3390/inorganics10100172>

Academic Editors: Bi-Xue Zhu and Chao Huang

Received: 22 September 2022

Accepted: 12 October 2022

Published: 14 October 2022

Publisher's Note: MDPI stays neutral with regard to jurisdictional claims in published maps and institutional affiliations.



Copyright: © 2022 by the authors. Licensee MDPI, Basel, Switzerland. This article is an open access article distributed under the terms and conditions of the Creative Commons Attribution (CC BY) license (<https://creativecommons.org/licenses/by/4.0/>).

1. Introduction

Both the thiosemicarbazones (TSCs) and their coordination compounds are well known to exhibit a broad spectrum of medicinal and agrochemical activities as antibacterial [1], antifungal [2,3], anticancer [4–6], antimalarial [7], and antitrypanosomal [8,9] agents. In particular, the Schiff base compounds involving the substitution of these nitrogen and sulfur bidentate ligands at their N1 position with heteroatom rings have been widely investigated as anticancer agents and their anticancer effects are mainly associated with the inhibition of the essential enzyme “ribonucleoside diphosphate reductase” that is involved in converting the ribonucleotides into deoxyribonucleotides amid DNA syntheses [10,11]. Triapine (3-aminopyridine-2-carboxaldehyde thiosemicarbazone) is a successful anticancer agent involved in clinical trials but it shows only a narrow spectrum of activity against specific cancerous cell types [10–13]. Further, a number of 2-acetylpyridine TSCs were also reported to possess significant toxicity against T87G, U87, and MCF-7 cancer cells with

insignificant toxicity in normal cells of red blood [14]. Indeed, several studies proved an improvement in the TSCs' biological activity upon complexation with metals providing a trustworthy strategy for dose reduction [1–3]. Gallium, copper, palladium, antimony, and tin complexes with TSCs of substituted pyridine were cytotoxic to human COLO-205, K-562, UACC-62, TK-10, MCF-7, HL-60, RT2, T98, and Jurkat cancer cells and their toxicities were high enough to cause the death of these cells by apoptosis [4–6,15,16]. Apart from the anti-cancer effects, several metal complexes of pyridine-2-carboxaldehyde TSCs proved good antifungal and antibacterial effects [17–22]. Structurally, the pyridine-2-carboxaldehyde TSCs are tridentate ligands producing highly stable coordination compounds, as these molecules bind the metals via one sulfur and two nitrogen atoms resulting in the metal involvement in two fused coplanar five-membered rings [17–22].

Antimony is a semimetal possessing a high affinity for coordination with sulfur and nitrogen donor ligands [9,23] and the antimony compounds are widely used as additives to lubricants and in industrial processes [24,25]. Antimony compounds are mainly used in medicine for the clinical treatment of parasitic infections, but they also show other biological activities [26–31]. Stimulated by the good performance of platinum anticancer agents, antimony compounds have been developed to show significant potential in tumor therapy [4]. Nowadays, there are antimony compounds proposed for the chemotherapy of acute promyelocytic leukemia (APL) [31]. Furthermore, antimony compounds have also shown potential antibacterial and antifungal activities [29].

Some of us previously demonstrated the synthesis of two tridentate TSCs ($\text{HL}^1 = 4-(2,4\text{-dimethylphenyl})-1-((2\text{-pyridinyl})\text{methylene})\text{thiosemicarbazide}$ and $\text{HL}^2 = 4-(2,5\text{-dimethoxyphenyl})-1-((2\text{-pyridinyl})\text{methylene})\text{thiosemicarbazide}$) together with their complexes with Mn(II), Ni(II), Cu(II), Zn(II), and Cd(II) and evaluated the antimicrobial activities of these compounds [17–20]. In continuation of this research, this paper exhibits studies on two new complexes of antimony as a main group element. The studies evaluate the in vitro anti-proliferative effect of the antimony complexes, compared with the standard (doxorubicin), against human breast MCF-7 cancer cells and baby hamster kidney (BHK) healthy cells. In addition to this, we also account for how the complexation with antimony enhanced the antifungal (against *Aspergillus flavus* and *Candida albicans*) and antibacterial (against *Staphylococcus aureus* and *Escherichia coli*) activities of the ligands and compare the obtained results with other data given by antifungal (amphotericin B) and antibacterial (ampicillin) standards.

2. Results and Discussion

2.1. Synthesis and Spectroscopic Characterization

The general structure of HL^1 [17] and HL^2 [18] is shown in Figure 1 and their synthetic procedures are present in detail in the respective literature. Briefly, the ligands were prepared in high yield via the addition of hydrazine hydrate to the respective substituted phenyl isothiocyanate (2,4-dimethylphenyl isothiocyanate for HL^1 and 2,5-dimethoxyphenyl isothiocyanate for HL^2) and condensation of the obtained thiosemicarbazides with pyridine-2-carboxaldehyde in the presence of a few drops of glacial acetic acid. The ligands were crystallized with aqueous ethanol and their purity was checked by elemental and spectroscopic analysis (FT-IR, $^1\text{H-NMR}$, and $^{13}\text{C-NMR}$).

Each $^1\text{H-NMR}$ spectrum of both ligands in DMSO-d_6 show two resonances, each integrated for three protons at 2.19 and 2.30 ppm for HL^1 and 3.72 and 3.85 ppm for HL^2 , corresponding to the methyl and methoxy protons, respectively. Both ligands show other three singlet peaks at 8.17, 10.04, and 11.95 ppm for HL^1 and 8.21, 10.10, and 12.16 ppm for HL^2 . These bands are, respectively, assigned to $\text{N} = \text{CH}(\text{azomethine})$, $\text{NH}(\text{thiourea})$, and $\text{NH}(\text{hydrazine})$ protons. Further, the $^1\text{H-NMR}$ spectrum of each ligand shows a set of one singlet, four doublet, and two triplet peaks ranging from 7.04 to 8.57 ppm for HL^1 and from 6.75 to 8.61 ppm for HL^2 , assigned to the ring protons.

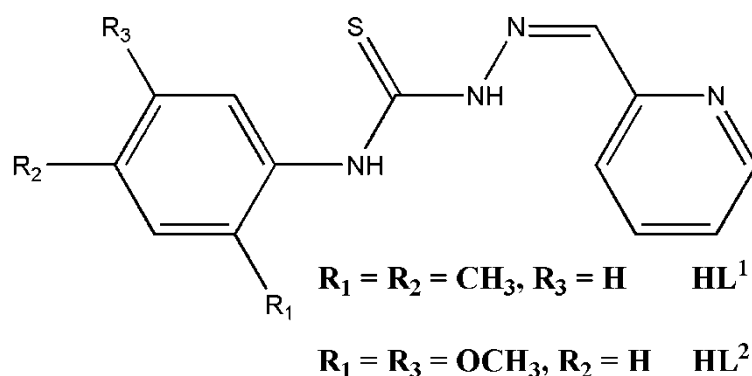


Figure 1. General structure of the thiosemicarbazone ligands.

The class of 2-formylpyridine TSCs has shown usefulness in coordinating several metal ions with a chelation mode via the imine (N), pyridine (N), and thiol (S) atoms in a monoanionic character [17–22]. These stable tridentate ligands at ambient temperature display thiol–thione tautomerism in the ligand solution [17–22]. The occurrence of the reactions between unimolar ratios of antimony trichloride and the ligands was in ethanol that after 1 h of stirring, the solids were isolated. The obtained trivalent antimony complexes were accessible in an acceptable yield of 65–91% and showed air and light stability as well as good room temperature solubility in a variety of common organic solvents, e.g., dichloromethane, acetone, DMF, and DMSO. Elemental analyses of carbon, hydrogen, nitrogen, and sulfur were performed and the results were in agreement with the theoretical values of 1:1 metal complexes (the general formula of $[Sb(L)Cl_2]$, $L = L^1$ or L^2 , was suspected for the complexes considering the monobasic nature of the ligands). In addition, negligible molar conductivities of 3.49 and 7.69 $\Omega^{-1}cm^2mol^{-1}$, respectively, for complexes **C1** and **C2** (10^{-3} M in DMF solutions) were determined revealing the molecular nature of the complexes [32].

The UV-Vis electronic absorption spectra of complexes **C1** and **C2** (10 μ M), recorded in dichloromethane, are not informative about their structures due to the absence of any charge transfer or metal-centered transitions in the spectra. Both ligands exhibited an absorption maximum at 322 nm for **HL¹** and 326 nm for **HL²**, and these maxima blueshifted to 321 nm in the spectra of the complexes. The tentative assignments of characteristic bands in the TSC ligands and their antimony complexes could be identified in their FT-IR spectra. The $\nu(^2NH)$ stretching vibrations, occurring at 3127 and 3136 cm^{-1} in the spectra of **HL¹** and **HL²**, respectively, disappeared for all complexes suggesting the coordination of the ligands in their deprotonated thiol form [18]. The infrared spectra of the ligands show distinct bands, attributed to thioamide vibrations [$\nu(CS) + \nu(CN)$], at 1372 and 868 cm^{-1} for **HL¹** and 1391 and 842 cm^{-1} for **HL²**. These bands exhibited redshifts to frequencies of 1307 and 837 cm^{-1} for **C1** and 1321 and 798 cm^{-1} for **C2**, supporting the antimony-sulfur bonding in the complexes [21]. The TSC 4NH groups were reported to contribute to hydrogen bonding resulting in the assembly of the compounds in polymeric chains [17]. Indeed, the respective stretching vibration of this group appears at 3222 cm^{-1} for **HL¹** and 3306 cm^{-1} for **HL²** and these bands underwent blueshift upon the antimony coordination suggesting strength differences in the hydrogen bonding between the ligands and their complexes [17]. The $\nu(C = N)$ vibrations appear at 1582 and 1606 cm^{-1} in the spectra of the ligands but experience a shift to the 1527–1530 cm^{-1} range in the spectra of **C1** and **C2** [20]. In addition to the latter band, the FT-IR spectra of **C1** and **C2** exhibit new bands associated with Sb—N(azomethine) bond vibrations in the range of 536–593 cm^{-1} [19]. Further, bands in the 1051–1078 cm^{-1} range owing to $\nu(N—N)$ vibrations in the ligands were shifted to the same bands appearing at 1119–1095 cm^{-1} in the spectra of the complexes [22]. The FT-IR spectra of the ligands show also bands at 621 and 405 cm^{-1} for **HL¹** and 622 and 407 cm^{-1} for **HL²**, assigned for in-plane and out-of-plane ring deformation vibrations [18]. The formation of

Sb—nitrogen(pyridine) bonds can be confirmed due to positive shifts of these bands to 635 and 444 cm^{-1} for **C1** and 647 and 441 cm^{-1} for **C2** in their respective spectra [21].

2.2. X-ray Crystallography

Refluxing the complex **C1** in methanol (200 mL) for six hours resulted in its dissolution and, upon cooling the solution in an ambient atmosphere, the formation of block-shaped orange X-ray quality crystals. A clear crystal with a size of $0.15 \times 0.11 \times 0.07 \text{ mm}^3$ of the complex was analyzed by X-ray crystallography. Figure 2 includes the crystal structure of complex **C1**. The complex packing scheme along the [100] direction is shown in Figure 3a,b, displaying the contact distance between two entities of **C1**. A summary of selected crystallographic and refinement data of the complex is depicted in Table 1 and selected geometric parameters (bond distances and angles in addition to hydrogen bonding information) of the complex are depicted in Table 2.

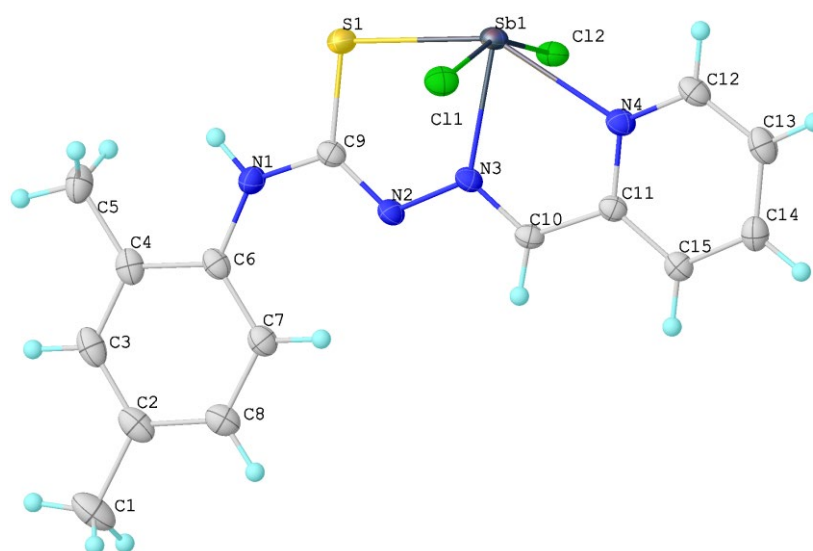


Figure 2. A molecular graphic of complex **C1** with thermal ellipsoids of 50 % probability level.

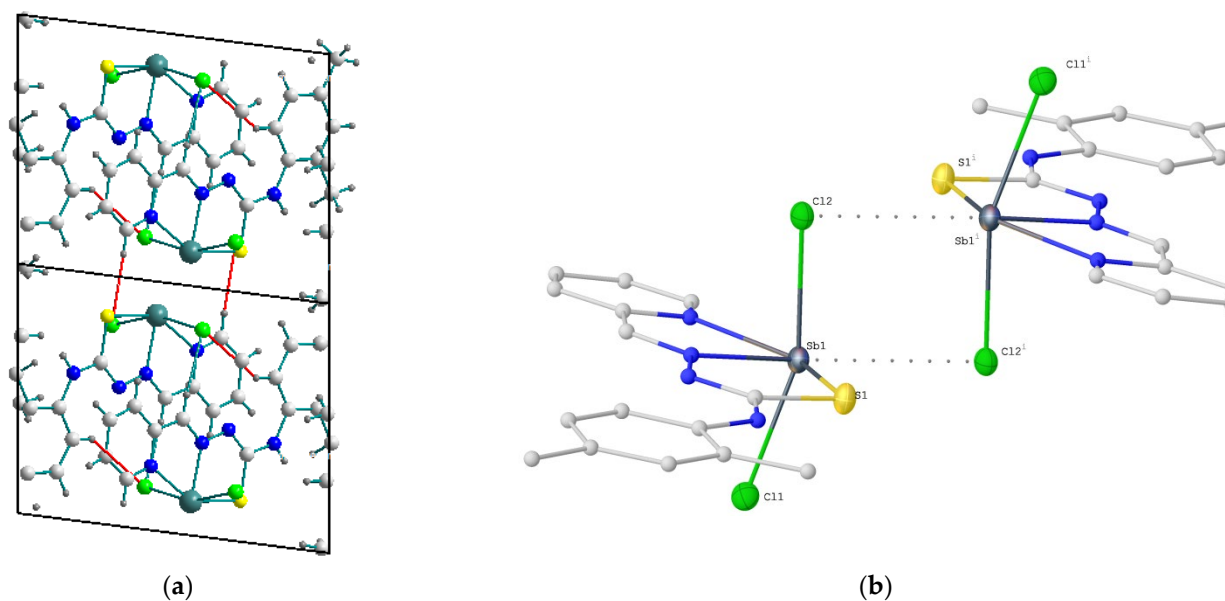


Figure 3. (a) The packing diagram of complex **C1** along crystallographic a-axis (red lines represent intermolecular H-interactions in the complex); (b) contacts of two entities of **C1** in the crystal packing. Ellipsoids are at 50 % probability level and X^i indicates symmetry-generated positions.

Table 1. Crystal data and structure refinement results for [Sb(L¹)Cl₂] C1.

Empirical formula	C ₁₅ H ₁₅ N ₄ SCl ₂ Sb	μ (mm ⁻¹)	16.395
Formula weight	476.04	F(000)	470.9
Crystal system	Triclinic	θ range for data collection (°)	3.81 to 73.95
Space group	P-1	Reflections collected	141,369
a (Å)	8.1520(1)	Unique refl. collected (R _{int})	3546 (0.0690)
b (Å)	9.3163(1)	Completeness to theta	100%
c (Å)	11.7748(1)	Parameters (Restraints)	210(0)
α (°)	82.279(1)	Max. and min. transmission	0.481 and 0.717
β (°)	83.243(1)	GOF on F ²	1.116
γ (°)	85.761(1)	R ₁ [I > 2 σ (I)]	0.0213 (3536)
Volume (Å ³)	878.457(16)	wR2 (all data)	0.0561
Z	2	Largest diff. peak, hole/e Å ⁻³	0.860 and -0.502
Density (g/cm ³)	1.800	CCDC number	2207805

Table 2. Selected bond lengths (Å), angles (°), and hydrogen bonding parameters (Å, °) for [Sb(L¹)Cl₂] C1.

Atoms	Distance (Å)	Atoms	Angle (°)	Atoms	Angle (°)
Sb1—Cl2	2.6048(6)	Cl2—Sb1—N4	83.69(5)	C11—N4—C12	118.8(2)
Sb1—Cl1	2.5786(6)	Cl1—Sb1—S1	92.12(2)	N3—C10—C11	119.8(2)
Sb1—S1	2.5215(6)	Cl1—Sb1—N3	80.90(5)	N3—C10—H10	120.1(3)
Sb1—N3	2.239(2)	Cl1—Sb1—N4	84.34(5)	S1—C9—N2	127.4(2)
Sb1—N4	2.410(2)	S1—Sb1—N3	76.43(5)	S1—C9—N1	113.6(2)
S1—C9	1.746(3)	S1—Sb1—N4	146.25(5)	N3—N2—C9	114.9(2)
N3—N2	1.372(3)	N3—Sb1—N4	69.86(6)	C6—N1—C9	132.0(2)
N3—C10	1.294(3)	Sb1—S1—C9	97.19(9)	C6—N1—H8	114.0(3)
N4—C11	1.350(3)	Sb1—N3—N2	123.9(1)	C9—N1—H8	114.0(3)
N4—C12	1.337(3)	Sb1—N3—C10	120.5(2)	N1—C6—C7	123.8(2)
N2—C9	1.311(4)	N2—N3—C10	115.7(2)	N1—C6—C4	116.0(2)
N1—C6	1.418(3)	Sb1—N4—C11	114.9(1)	N2—C9—N1	118.9(2)
N1—C9	1.361(3)	Sb1—N4—C12	126.3(2)	C8—C2—C1	120.7(2)
Hydrogen bonding interaction parameters					
D—H ... A	d(D—H)	d(H ... A)	d(D ... A)	<(D—H ... A)	
C7—H7 ... Cl2 ⁽ⁱ⁾	0.930(4)	2.8608(3)	3.6137(3)	138.927(2)	
C12—H12 ... Cl1 ⁽ⁱⁱ⁾	0.930(4)	2.7470(3)	3.6692(3)	171.218(3)	
(i) 1 - x, 1 - y, 1 - z		(ii) 2 - x, -y, 1 - z			

The complex crystallizes in the P-1 triclinic space group, where its asymmetric unit is represented by an entire complex molecule. In the complex, each Sb(III) ion is surrounded by a pyridine nitrogen (N4) atom, an azomethine nitrogen (N3) atom, and a thiol sulfur (S1) atom all from the TSC ligand anion with an angle of 146.25(5)° [S1—Sb1—N4] indicating slight deviation of the Sb1 atom from the NNS plane. This chelation provided two almost coplanar fused five-membered chelate rings with a centroid-centroid distance of 2.320 Å and torsion angles of 176.3(2)° [S1—Sb1—N3—C10] and 177.9(2)° [N4—Sb1—N3—N2]. The trivalent antimony in the complex is further ligated by two chlorine atoms (Cl2 and Cl1) that both exist in an almost *trans*-arrangement with Cl2—Sb1—Cl1 angle of 159.82(2)°. This means the presence of a pseudo-octahedral geometry around the trivalent antimony with Cl2, Cl1, N4, S1, and N3 sites in addition to a pair of electrons (5 s²) found in the configuration of the trivalent antimony.

By some of us, the crystal structure of HL¹ has been previously determined with synchrotron X-ray powder diffraction [17]. As expected, the C9—S1 bond distance which is 1.6702 Å in HL¹ goes to 1.746(3) Å in C1. This lengthening is due to a variation in the bond order, which has a double bond character in the free ligand and a predominantly single bond character in the antimony complex. Similarly, the N2—C9 bond distance varies from

1.3859 Å in the free TSC to 1.311(4) Å in **C1** due to this same effect. Indeed, this effect results from deprotonation at N2 and the consequent formation of a highly delocalized system along the ligand. Further, to match the steric requirements of tridentate coordination, the bond angles undergo important changes in coordination: the N3—N2—C9 angle goes from 122.81° in **HL**¹ to 114.9(2)° in **C1**, N2—C9—S1 varies from 117.05° in **HL**¹ to 127.4(2)° in **C1**, N1—C9—S1 goes from 130.41° in **HL**¹ to 113.6(2)° in **C1**, and C10—N3—N2 goes from 117.67° in **HL**¹ to 115.7(2)° in **C1**.

The distances and angles in complex **C1** are comparable with two other antimony complexes with the ligands {2-acetylpyridine-N(4)-orthochlorophenyl thiosemicarbazone and 2-acetylpyridine-N(4)-ortho-fluorophenyl thiosemicarbazone} [9]. The angle Cl2—Sb1—Cl1 in complex **C1** is 159.82(2)° in agreement with the values of 162.67(3) and 162.59(3) Å reported for similar angles [9]. The small chelate bite angles N4—Sb1—N3 {69.86(6) Å} and N3—Sb1—S1 {76.43(5) Å} in complex **C1** deviate significantly from the value of 90° clearing some distortion from the ideal pseudo-octahedral arrangement. These deviations, which are due to probable spatial requirements of the ligand chelating system, are in close proximity to values in the ranges of 69.44(9)°–69.31(9)° and 76.51(6)°–76.42(7)° reported for related angles in the literature [9].

In the structure, the two Sb(III)—Cl distances {2.6048(6) and 2.5786(6) Å} are longer than the Sb(III)—S bond {2.5215(6) Å}. Furthermore, slight shortening exists between the distance of Sb(III)—N(azomethine) {2.239(2) Å} and that of Sb(III)—N(pyridine) {2.410(2) Å} and this shortening was observed for other trivalent antimony complexes with tridentate TSCs [9]. In the crystal packing, intermolecular H-bonds (Table 2) were also detected resulting in the layered structure of the complex with two alternated distances between each pair of similar atoms. Indeed, every two entities of **C1** are in close contact with an intermolecular Sb1—Cl2 distance of 3.261(6) Å and an Sb—Sb distance of 4.2404(4) Å, while the closest S—S distance is 5.5080(11) Å.

2.3. Antibacterial and Antifungal Activity Screening

Figure 4 presents the antibacterial assay results of **HL**¹, **HL**², **C1**, **C2**, and the standard drug ampicillin (20 mg/mL) against two bacterial strains (G +ve (*Staphylococcus aureus*) and G -ve (*Escherichia coli*)) obtained via the Kirby–Bauer diffusion method [33]. Interestingly, improvement in the inhibitory effect on the bacteria by the complexes, due to the impact of the central antimony, in comparison to that by the ligands and the antibacterial reference was detected. In more detail, the results indicate inhibitions of 21 and 25 mm, respectively, against *Staphylococcus aureus* and *Escherichia coli* given by the ampicillin standard. On the other hand, the coordinated Sb(III) ion increased the activity of **HL**¹ and **HL**²; the compounds **HL**¹, **HL**², **C1**, and **C2** showed, respectively, inhibitions of 14, 10, 36, and 32 mm against *Staphylococcus aureus* and 15, 10, 35, and 31 mm against *Escherichia coli*. This means the ligands showed lower antibacterial activities than ampicillin but the complexation with antimony enhanced the antibacterial effects of the ligands to exceed the standard. These results agree with the literature [34] that indicates high antibacterial activity by trivalent antimony complexes of tosyl-sulfonamides against both *Staphylococcus aureus* and *Escherichia coli* cultures.

The same concentration of all compounds (20 mg/mL) was also used to screen whether it gives inhibition to fungal species or not (Figure 5). Hence, the antifungal activities were determined against *Aspergillus flavus* and *Candida albicans*, where amphotericin B was used as a drug reference. It is worth noting that all ligands and complexes possessed no effect against *Aspergillus flavus*; however, only **HL**¹ inhibited the growth of *Candida albicans* by 10 mm, and interestingly, its derived complex **C1** showed fungal inhibition of 21 mm, which is the same inhibition displayed by the reference drug.

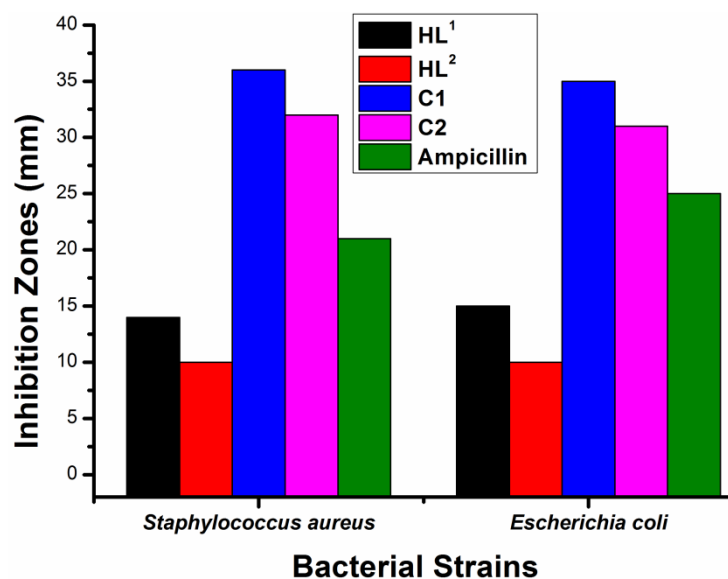


Figure 4. Antibacterial inhibitory effects, as the inhibition zone diameters (mm) displayed by ampicillin in addition to the TSC ligands and complexes, against two bacterial strains (*Staphylococcus aureus* and *Escherichia coli*).

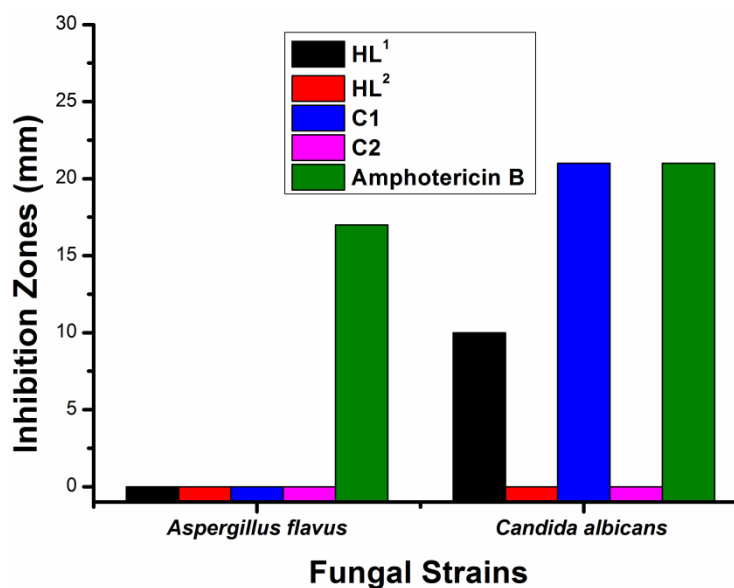


Figure 5. Antifungal inhibitory effects, as the inhibition zone diameters (mm), against *Aspergillus flavus* and *Candida albicans*, caused by ligands (HL¹ and HL²), complexes (C1 and C2), and amphotericin B.

To conclude, it is clear that complexation with trivalent antimony enhanced the antimicrobial effect of the ligands to the limit that exceeded the effect of the antibacterial standard and that, often, equaled the effect of the antifungal reference. Indeed, for the enhancement in the bioactivity profile of ligands in coordination with metals, it was previously documented that bioactive ligands could improve their bioactivities and inactive ligands could attain pharmacological properties [35,36]. In addition, it is well known that metal coordination is an efficient strategy in designing slow-release and long-acting chemotherapeutics [35,36].

2.4. Cytotoxicity in Cancer and Normal Cells

Breast cancer is currently considered the cancer type with the highest degree of incidence among women worldwide and the epithelial-adenocarcinoma MCF-7 cells have

been utilized as model cells for this type of cancer [28]. In this work, the SRB assay method was applied instead of the MTT assay. This is because direct interference in the results could be obtained from the MTT method due to MTT reduction even if cell viability is not affected [37]. The cytotoxic activities of 0–100 $\mu\text{g}/\text{mL}$ of the free TSCs and their antimony complexes (C1 and C2) against MCF-7 human breast cancer cell lines were assayed (Figure 6a). Generally, the cells were found less sensitive to the ligands in comparison to the derived complexes, as the compound concentrations in DMSO required to inhibit 50 % of MCF-7 cells were 68.9, 145.4, 34.7, and 37.4 μM for HL¹, HL², C1, and C2, respectively. These results indicate greater activity for the dimethyl-substituted ligand and its complex and the activity differences might be owing to various expression levels of anti-apoptotic proteins in the tumor, in addition to other multifactorial mechanisms of drug resistance by the cells [4]. It is worth mentioning that doxorubicin gave an IC₅₀ value of 9.66 μM clearing higher activity for the standard drug than HL¹ (IC₅₀ = 68.9 μM), HL² (IC₅₀ = 145.4 μM), C1 (IC₅₀ = 34.7 μM), and C2 (IC₅₀ = 37.4 μM).

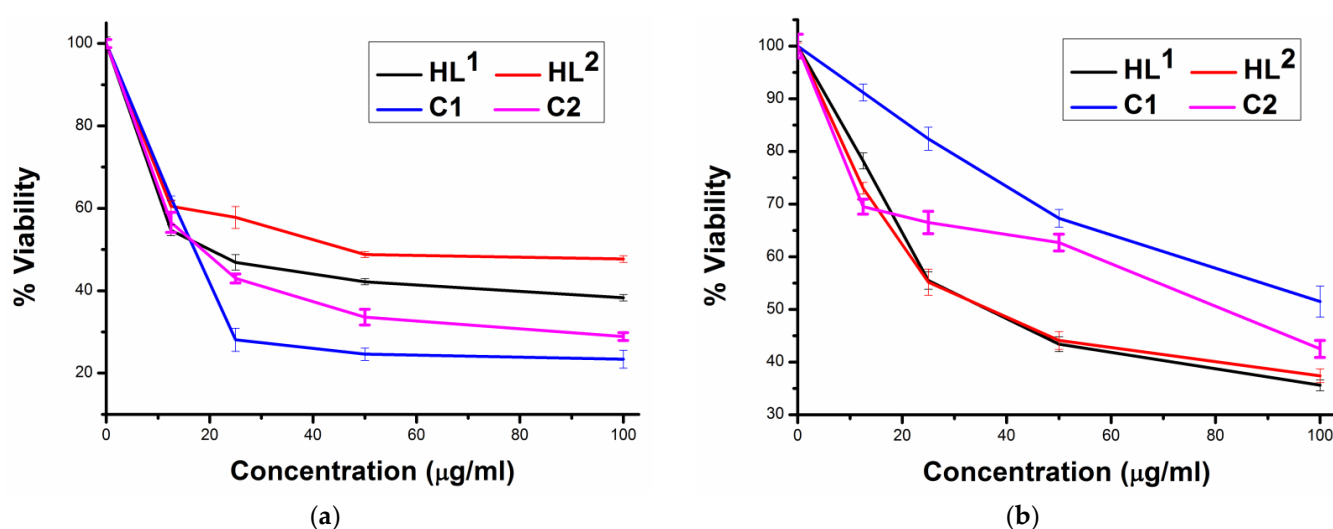


Figure 6. Relative anti-proliferative activities displayed by HL¹, HL², C1, and C2 (0–100 $\mu\text{g}/\text{mL}$): (a) against MCF-7 cancer, and (b) against BHK healthy cells.

On another hand, whenever an anticancer activity is measured, the cytotoxic effect of the compounds on the healthy cells (Figure 6b) should also be determined to ensure the selectivity of the compounds against the cancer cells. Here, we examined the effect of all ligands, coordination compounds, and doxorubicin against healthy baby hamster kidney (BHK) cells and, interestingly, determined the greatest toxicity with an IC₅₀ value of 36.42 μM for doxorubicin. This is while HL¹ and HL² exhibited lower toxicities, respectively, with IC₅₀ = 126.6 and 110.6 μM . Finally, the complexes C1 and C2 (100 $\mu\text{g}/\text{mL}$: 210.1 μM of C1 and 196.8 μM of C2) gave surviving fractions of 51.5% and 42.5% (IC₅₀ = 160.6 μM) of BHK cells indicating very low toxicity in the normal BHK cells by the complexes compared with HL¹, HL², and doxorubicin.

3. Materials and Methods

3.1. Chemicals and Instruments

If not mentioned otherwise, all experimental work was conducted at ambient room temperature in the air. Analytical grade chemicals {2,4-dimethylphenyl isothiocyanate (Alfa Aesar), 2,5-dimethoxyphenyl isothiocyanate (Sigma-Aldrich), hydrazine hydrate (Sigma-Aldrich), and pyridine-2-carboxaldehyde (Alfa-Aesar)} were purchased. In addition to commercially supplied glacial acetic acid, these chemicals were used as received for the preparation of the ligands [17,18]. Antimony trichloride was purchased from MERCK (Germany). The nuclear magnetic resonance spectra in DMSO-d₆ were taken on a Bruker 400 MHz spectrometer (tetramethylsilane (TMS) acted as the internal reference). Elemental

data were generated with a Vario EL III CHNS Element Analyzer. A Jenway 4320 conductivity meter estimated the electrical conductivity of the complexes in DMF solutions. UV-visible spectral data for all compounds in dichloromethane were collected on a Perkin-Elmer Lambda 40 UV/VIS spectrometer and their infrared spectral data as KBr pellets were taken using a Nicolet iS10 FT-IR Spectrometer.

3.2. Single Crystal X-ray Diffraction Analysis

Data for complex **C1** were obtained at 123.00 (10) K from a single crystal of the complex mounted on a MITIGEN holder in per-fluoro-ether oil on a Rigaku Oxford Diffraction SuperNova, TitanS2 diffractometer. CuK α radiation ($\lambda = 1.54184 \text{ \AA}$) was generated and the data were collected using ω scans. The diffraction pattern was indexed and the total number of runs and images was based on the strategy calculation from the program CrysAlisPro (Rigaku, V1.171.41.21a, 2019) [38]. The unit cell was refined using CrysAlisPro (Rigaku, V1.171.41.21a, 2019) on 37,435 reflections and the same program was used for data reduction, scaling, and absorption corrections [38]. A Gaussian absorption correction was performed and numerical absorption correction was applied based on Gaussian integration over a multifaceted crystal model [38]. Empirical absorption correction using spherical harmonics was implemented in the SCALE3 ABSPACK scaling algorithm [32]. The structure was solved with the ShelXT 2018/2 structure solution program [39] using dual methods and Olex2 as the graphical interface [39]. The model was refined using full matrix least squares minimization on F^2 using a version of olex2.refine 1.5-alpha [40,41]. The non-hydrogen atoms were anisotropically refined, while the hydrogen atom positions were calculated geometrically from the difference Fourier map and refined using the riding model. ORTEP-3 [42] and DIAMOND [43] software were used for drawing the molecular graphic and packing diagram of the complex **C1**, respectively.

3.3. Preparation of the Complexes

The appropriate ligand (100 mg; 0.352 mmol of **HL**¹ or 0.316 mmol of **HL**²) was dissolved in ethanol ($\approx 20 \text{ mL}$) and an equivalent of antimony trichloride (72–80 mg, 0.316–0.352 mmol) was added with stirring. The mixtures were stirred for an hour before filtering the solids, washing them with ethanol and diethyl ether, and drying them in the air.

[Sb(L¹)Cl₂] **C1**: Yield = 109 mg (65%). Anal. Calcd. (Found) for C₁₅H₁₅N₄SCl₂Sb (MW = 476.04 g/mol), C = 37.85 (38.09)%, H = 3.18 (3.24)%, N = 11.77 (11.91)%, and S = 6.74 (6.67)%. FT-IR (KBr, cm⁻¹) = 3325 ν (⁴NH), 1527 ν (C = N), 1307–837 [ν (CS) + ν (CN)], 1119 ν (N–N), 635 Py(iP), 536 ν (Sb–N_{azomethine}), and 444 Py(OP). UV-Visible (dichloromethane, nm) = 321. Molar conductance (DMF, $\Omega^{-1}\text{cm}^2\text{mol}^{-1}$) = 3.49.

[Sb(L²)Cl₂] **C2**: Yield = 147 mg (91%). Anal. Calcd. (Found) for C₁₅H₁₅N₄SO₂Cl₂Sb (MW = 508.04 g/mol), C = 35.46 (35.50)%, H = 2.98 (2.81)%, N = 11.03 (11.55)%, and S = 6.31 (6.38)%. FT-IR (KBr, cm⁻¹) = 3341 ν (⁴NH), 1530 ν (C = N), 1321–798 [ν (CS) + ν (CN)], 1095 ν (N–N), 647 Py(iP), 593 ν (Sb–N_{azomethine}), and 441 Py(OP). UV-Visible (dichloromethane, nm) = 321. Molar conductance (DMF, $\Omega^{-1}\text{cm}^2\text{mol}^{-1}$) = 7.69.

3.4. Evaluation of Antibacterial and Antifungal Activities

The synthesized ligands and complexes were screened for in vitro antimicrobial activities against the bacteria (*Staphylococcus aureus* ATCC 12,600 and *Escherichia coli* ATCC 11775) and fungi (*Aspergillus flavus* ATCC 9643 and *Candida albicans* ATCC 10231) in comparison to ampicillin (antibacterial reference) and amphotericin B (antifungal reference) using the modified Kirby–Bauer disc diffusion method [33]. The obtained bacterial isolates were maintained on broth nutrient agars and the fungal isolates were maintained on Sabouraud Dextrose (SD) agars. From each isolate, one hundred microliters were transferred to grow in 10 mL of fresh media until reaching an approximate count of 5×10^8 microorganisms/mL (for *Staphylococcus aureus* and *Escherichia coli*), 5×10^3 microorganisms/mL (for *Aspergillus flavus*), and 5×10^5 microorganisms/mL (for *Candida albicans*). From each culture, microbial suspension (100 μL) was spread onto each agar plate similar in composition to the

broth in which the isolates were maintained. *Aspergillus flavus* plates were incubated at 25 °C for 48 h, *Candida albicans* plates were incubated at 30 °C for 48 h, and the bacterial plates (*Staphylococcus aureus* and *Escherichia coli*) were incubated at 37 °C for 24 h. The antimicrobial agents (HL¹, HL², C1, C2, ampicillin, and amphotericin B) were dissolved in DMSO (20 mg/mL) and 8.0 mm diameter blank paper discs (Schleicher and Schuell, Spain) were impregnated with 10 µL from each solution. Placing the filter paper discs on the microbial agars caused microbial inhibition around the discs. The area diameters of no microbial growth around the discs (i.e., the inhibition zones) were measured with a slipping caliper of the National Committee for Clinical Laboratory Standards. The solvent DMSO exhibited no inhibitory effect on the tested microorganisms.

3.5. Cytotoxicity against MCF-7 Cancer and BHK Normal Cells

The cytotoxicity of the ligands and their complexes C1 and C2, as well as the standard “doxorubicin” against human breast adenocarcinoma (MCF-7), and normal baby hamster kidney (BHK) cells obtained from the American Tissue Culture Collection (ATCC, Minnesota, USA) has been evaluated [37]. The cells were maintained in the National Cancer Institute (Cairo, Egypt) by serial sub-culturing. The cells were seeded into 96-well microtiter plates (4000 cells/well in 200 µL of fresh medium) at 37 °C and [CO₂] < 5%. On the following day, a stock solution of each substance was freshly prepared in DMSO and diluted to form solutions of 0, 12.5, 25, 50, and 100 µg/mL of each compound. After the solutions were added to the plates and incubated for 48 h in a CO₂ incubator, the cultures were fixed at 4 °C via layering fifty microliters of cold trichloroacetic acid (50%) on each well. The cultures were then washed with distilled water and sulphorhodamine-B (SRB, 0.4%, 50 µL) solution in 1% acetic acid was added for staining the cultures for 30 min in the dark at an ambient temperature. The plates were afterward rewashed with acetic acid (1%) and dried in the air. TRIS base (10 mM, pH 10.5, 200 µL per well) was added to solubilize the dye. The absorbance in each well was then measured at 570 nm with the help of an ELISA microplate reader (Sunrise Tecan reader, Germany). Parallel with each measurement, the absorbance in a control plate containing no anticancer compound is considered to correspond to a 100% surviving fraction. The percent viability corresponding to each concentration was calculated using the mean absorbance value of three replicates.

4. Conclusions

Two antimony(III) complexes with tridentate thiosemicarbazone NNS donor atom ligands were prepared so that the ligands reacted monoanionic and pseudo-octahedral geometry, which was investigated around the central semimetal. The complexes displayed great antibacterial effects against *S. aureus* and *E. coli* more than the effects by the ligands and even by the standard. Further, only one complex inhibited the growth of *C. albicans* with the same inhibition given by amphotericin B. The anti-proliferative activity of the ligands against MCF-7 human breast cancer cells enhanced after their coordination but the enhancement is not greater than that of doxorubicin. However, the activities shown by all compounds against BHK healthy cells followed this trend (doxorubicin > the ligands > the complexes), indicating the lowest toxicities by the complexes compared with the standard. In conclusion, the antimony complexes in this study gave excellent antibacterial and good anticancer activities in addition to insignificant toxicity in normal cells compared with standards.

Author Contributions: Conceptualization, A.B.M.I., S.A.E. and S.M.A.; methodology, A.F., A.B.M.I., F.M., M.B. and S.M.A.; crystal structure analysis, F.M. and M.B.; investigation, A.F., A.B.M.I. and S.M.A.; writing-original draft preparation, A.B.M.I.; writing-review and editing, A.F., A.B.M.I., S.A.E., F.M., M.B. and S.M.A.; visualization, A.B.M.I., F.M. and M.B.; supervision, A.B.M.I., S.A.E. and S.M.A. All authors have read and agreed to the published version of the manuscript.

Funding: This research received no external funding.

Data Availability Statement: The complex C1 crystallographic data have been deposited with the Cambridge Crystallographic Data Centre (CCDC-2207805). Data on this structure can be obtained free of charge from <https://www.ccdc.cam.ac.uk/structures/>, access on 20 September 2022.

Conflicts of Interest: The authors declare no conflict of interest.

References

1. Da Silva, J.G.; Azzolini, L.S.; Wardell, S.M.S.V.; Wardell, J.L.; Beraldo, H. Increasing the antibacterial activity of gallium(III) against *Pseudomonas aeruginosa* upon coordination to pyridine-derived thiosemicarbazones. *Polyhedron* **2009**, *28*, 2301–2305. [CrossRef]
2. Mendes, I.C.; Moreira, J.P.; Ardisson, J.D.; Dos Santos, R.G.; Da Silva, P.R.O.; Garcia, I.; Castiñeiras, A.; Beraldo, H. Organotin(IV) complexes of 2-pyridineformamide-derived thiosemicarbazones: Antimicrobial and cytotoxic effects. *Eur. J. Med. Chem.* **2008**, *43*, 1454–1461. [CrossRef] [PubMed]
3. Parrilha, G.L.; Da Silva, J.G.; Gouveia, L.F.; Gasparoto, A.K.; Dias, R.P.; Rocha, W.R.; Santos, D.A.; Speziali, N.L.; Beraldo, H. Pyridine-derived thiosemicarbazones and their tin(IV) complexes with antifungal activity against *Candida* spp. *Eur. J. Med. Chem.* **2011**, *46*, 1473–1482. [CrossRef]
4. Reis, D.C.; Pinto, M.C.X.; Souza-Fagundes, E.M.; Wardell, S.M.S.V.; Wardell, J.L.; Beraldo, H. Antimony(III) complexes with 2-benzoylpyridine-derived thiosemicarbazones: Cytotoxicity against human leukemia cell lines. *Eur. J. Med. Chem.* **2010**, *45*, 3904–3910. [CrossRef] [PubMed]
5. Pathan, A.H.; Ramesh, A.K.; Bakale, R.P.; Naik, G.N.; Kumar, H.G.R.; Frampton, C.S.; Rao, G.M.A.; Gudasi, K.B. Association of late transition metal complexes with ethyl 2-(2-(4-chlorophenylcarbamothioyl)hydrazono)propanoate: Design, synthesis and in vitro anticancer studies. *Inorg. Chim. Acta* **2015**, *430*, 216–224. [CrossRef]
6. Mendes, I.C.; Soares, M.A.; Dos Santos, R.G.; Pinheiro, C.; Beraldo, H. Gallium(III) complexes of 2-pyridineformamide thiosemicarbazones: Cytotoxic activity against malignant glioblastoma. *Eur. J. Med. Chem.* **2009**, *44*, 1870–1877. [CrossRef] [PubMed]
7. Klayman, D.L.; Bartosevich, J.F.; Griffin, T.S.; Mason, C.J.; Scovill, J.P. 2-Acetylpyridine thiosemicarbazones. 1. A new class of potential antimalarial agents. *J. Med. Chem.* **1979**, *22*, 855–862. [CrossRef]
8. Merlino, A.; Benitez, D.; Chavez, S.; Da Cunha, J.; Hernandez, P.; Tinoco, L.W.; Campillo, N.E.; Paez, J.A.; Cerecetto, H.; Gonzalez, M. Development of second generation amidinohydrazone, thio- and semicarbazones as *Trypanosoma cruzi*-inhibitors bearing benzofuroxan and benzimidazole 1,3-dioxide core scaffolds. *Med. Chem. Commun.* **2010**, *1*, 216–228. [CrossRef]
9. Parrilha, G.L.; Dias, R.P.; Rocha, W.R.; Mendes, I.C.; Benítez, D.; Varela, J.; Cerecetto, H.; Gonzalez, M.; Melo, C.M.L.; Neves, J.K.A.L.; et al. 2-Acetylpyridine- and 2-benzoylpyridine-derived thiosemicarbazones and their antimony(III) complexes exhibit high anti-trypanosomal activity. *Polyhedron* **2012**, *31*, 614–621. [CrossRef]
10. Finch, R.A.; Liu, M.C.; Grill, S.P.; Rose, W.C.; Loomis, R.; Vasquez, K.M.; Cheng, Y.C.; Sartorelli, A.C. Triapine (3-aminopyridine-2-carboxaldehyde-thiosemicarbazone): A potent inhibitor of ribonucleotide reductase activity with broad spectrum antitumor activity. *Biochem. Pharmacol.* **2000**, *59*, 983–991. [CrossRef]
11. Gojo, I.; Tidwell, M.L.; Greer, J.; Takebe, N.; Seiter, K.; Pochron, M.F.; Johnson, B.; Sznol, M.; Karp, J.E. Phase I and pharmacokinetic study of Triapine[®], a potent ribonucleotide reductase inhibitor, in adults with advanced hematologic malignancies. *Leuk. Res.* **2007**, *31*, 1165–1173. [CrossRef] [PubMed]
12. Wadler, S.; Makower, D.; Clairmont, C.; Lambert, P.; Fehn, K.; Sznol, M. Phase I and pharmacokinetic study of the ribonucleotide reductase inhibitor, 3-aminopyridine-2-carboxaldehyde thiosemicarbazone, administered by 96-h intravenous continuous infusion. *J. Clin. Oncol.* **2004**, *22*, 1553–1563. [CrossRef] [PubMed]
13. Karp, J.E.; Giles, F.J.; Gojo, I.; Morris, L.; Greer, J.; Johnson, B.; Thein, M.; Sznol, M.; Low, J. A Phase I study of the novel ribonucleotide reductase inhibitor 3-aminopyridine-2-carboxaldehyde thiosemicarbazone (3-AP, Triapine[®]) in combination with the nucleoside analog fludarabine for patients with refractory acute leukemias and aggressive myeloproliferative disorders. *Leuk. Res.* **2008**, *32*, 71–77. [PubMed]
14. Soares, M.A.; Lessa, J.A.; Mendes, I.C.; Da Silva, J.G.; Dos Santos, R.G.; Salum, L.B.; Daghestani, H.; Andricopulo, A.D.; Day, B.W.; Vogt, A.; et al. N⁴-Phenyl-substituted 2-acetylpyridine thiosemicarbazones: Cytotoxicity against human tumor cells, structure-activity relationship studies and investigation on the mechanism of action. *Bioorg. Med. Chem.* **2012**, *20*, 3396–3409. [CrossRef] [PubMed]
15. Rebolledo, A.P.; Ayala, J.D.; Lima, G.M.; Marchini, N.; Bombieri, G.; Zani, C.L.; Souza-Fagundes, E.M.; Beraldo, H. Structural studies and cytotoxic activity of N(4)-phenyl-2-benzoylpyridine thiosemicarbazone Sn(IV) complexes. *Eur. J. Med. Chem.* **2005**, *40*, 467–472. [CrossRef]
16. Rebolledo, A.P.; Vieites, M.; Gambino, D.; Piro, O.E.; Castellano, E.E.; Zani, C.L.; Fagundes, E.M.S.; Teixeira, L.R.; Batista, A.A.; Beraldo, H. Palladium(II) complexes of 2-benzoylpyridine-derived thiosemicarbazones: Spectral characterization, structural studies and cytotoxic activity. *J. Inorg. Biochem.* **2005**, *99*, 698–706. [CrossRef]
17. Ibrahim, A.B.M.; Farh, M.K.; Plaisier, J.R.; Shalaby, E.M. Synthesis, structural and antimicrobial studies of binary and ternary complexes of a new tridentate thiosemicarbazone. *Future Med. Chem.* **2018**, *10*, 2507–2519. [CrossRef]
18. Ibrahim, A.B.M.; Farh, M.K.; Mayer, P. Copper complexes of new thiosemicarbazone ligands: Synthesis, structural studies and antimicrobial activity. *Inorg. Chem. Commun.* **2018**, *94*, 127–132. [CrossRef]

19. Ibrahim, A.B.M.; Farh, M.K.; Mayer, P. Synthesis, structural studies and antimicrobial evaluation of nickel (II) complexes of NNS tridentate thiosemicarbazone based ligands. *Appl. Organomet. Chem.* **2019**, *33*, e4883. [[CrossRef](#)]
20. Ibrahim, A.B.M.; Farh, M.K.; Santos, I.C.; Paulo, A. Nickel Complexes Bearing SNN and SS Donor Atom Ligands: Synthesis, Structural Characterization and Biological activity. *Appl. Organomet. Chem.* **2019**, *33*, e5088. [[CrossRef](#)]
21. Ibrahim, A.B.M.; Farh, M.K.; El-Gyar, S.A.; EL-Gahami, M.A.; Fouad, D.M.; Silva, F.; Santos, I.C.; Paulo, A. Synthesis, structural studies and antimicrobial activities of manganese, nickel and copper complexes of two new tridentate 2-formylpyridine thiosemicarbazone ligands. *Inorg. Chem. Commun.* **2018**, *96*, 194–201. [[CrossRef](#)]
22. Mahmoud, G.A.-E.; Ibrahim, A.B.M.; Mayer, P. Zn(II) and Cd(II) thiosemicarbazones for stimulation/inhibition of kojic acid biosynthesis from *Aspergillus flavus* and the fungal defense behavior against the metal complexes' excesses. *J. Biol. Inorg. Chem.* **2020**, *25*, 797–809. [[CrossRef](#)]
23. Demicheli, C.; Ochoa, R.; Da Silva, J.B.B.; Falcao, C.A.B.; Rossi-Bergmann, B.; de Melo, A.L.; Sinisterra, R.D.; Frezard, F. Oral delivery of meglumine antimoniate- β -cyclodextrin complex for treatment of leishmaniasis. *Antimicrob. Agents Chemother.* **2004**, *48*, 100–103. [[CrossRef](#)] [[PubMed](#)]
24. Gencarelli, R.A.; Hughes, K.A.; Sierakowski, J.F. Extreme Pressure Additive for Lubricants. U.S. Patent 3988249A, 26 October 1976.
25. Willingham, G.L. Use of Antimony Salt Stabilizers for 3-Isothiazolones. U.S. Patent 5145981A, 8 September 1992.
26. Ozturk, I.I.; Yazar, S.; Gürkan, M.; Ceyhan, D.; Banti, C.N.; Hadjidakou, S.K.; Manoli, M.; Moushi, E.; Tasiopoulos, A.J. Synthesis, characterization and biological evaluation of novel antimony(III) iodide complexes with tetramethylthiourea and N-ethylthiourea. *Inorg. Chim. Acta* **2019**, *491*, 14–24. [[CrossRef](#)]
27. Duffin, J.; Campling, B.G. Therapy and disease concepts: The history (and future?) of antimony in cancer. *J. Hist. Med. Allied Sci.* **2002**, *57*, 61–78. [[CrossRef](#)] [[PubMed](#)]
28. Hadjidakou, S.K.; Ozturk, I.I.; Banti, C.N.; Kourkoumelis, N.; Hadjiliadis, N. Recent advances on antimony(III/V) compounds with potential activity against tumor cells. *J. Inorg. Biochem.* **2015**, *153*, 293–305. [[CrossRef](#)]
29. Tripathi, U.N.; Solanki, J.S.; Ahmad, M.S.; Bhardwaj, A. Synthesis, spectral and antimicrobial studies of chloroantimony(III)di [3(2'-hydroxyphenyl)-5-(4-substitutedphenyl)pyrazolines]. *J. Coord. Chem.* **2009**, *62*, 636–644. [[CrossRef](#)]
30. Ozturk, I.I.; Banti, C.N.; Manos, M.J.; Tasiopoulos, A.J.; Kourkoumelis, N.; Charalabopoulos, K.; Hadjidakou, S.K. Synthesis, characterization and biological studies of new antimony(III) halide complexes with ω -thiocaprolactam. *J. Inorg. Biochem.* **2012**, *109*, 57–65. [[CrossRef](#)]
31. Sharma, P.; Perez, D.; Cabrera, A.; Rosas, N.; Arias, J.L. Perspectives of antimony compounds in oncology. *Acta Pharmacol. Sin.* **2008**, *29*, 881–890. [[CrossRef](#)]
32. Geary, W.J. The use of conductivity measurements in organic solvents for the characterization of coordination compounds. *Coord. Chem. Rev.* **1971**, *7*, 81–122. [[CrossRef](#)]
33. Fekete, T.; Tumah, H.; Woodwell, J.; Truant, A.; Satischandran, V.; Axelrod, P.; Kreter, B. A comparison of serial plate agar dilution, bauer-kirby disk diffusion, and the vitek automicrobic system for the determination of susceptibilities of *Klebsiella* spp., *Enterobacter* spp., and *Pseudomonas aeruginosa* to ten antimicrobial agents. *Diagn. Microbiol. Infect. Dis.* **1994**, *18*, 251–258. [[CrossRef](#)]
34. Khan, N.U.H.; Nadeem, K.S.H. Synthesis, characterization and antibacterial activity of new antimony (III) complexes of some tosyl-sulfonamide derivatives. *Middle East J. Sci. Res.* **2013**, *16*, 1109–1115.
35. Abdolmaleki, S.; Yarmohammadi, N.; Adibi, H.; Ghadermazi, M.; Ashengroph, M.; Rudbari, H.A.; Bruno, G. Synthesis, X-ray studies, electrochemical properties, evaluation as in vitro cytotoxic and antibacterial agents of two antimony (III) complexes with dipicolinic acid. *Polyhedron* **2019**, *159*, 239–250. [[CrossRef](#)]
36. Ferraz, K.S.O.; Silva, N.F.; da Silva, J.G.; de Miranda, L.F.; Romeiro, C.F.D.; Souza-Fagundes, E.M.; Mendes, I.C.; Beraldo, H. Investigation on the pharmacological profile of 2,6-diacetylpyridine bis(benzoylhydrazone) derivatives and their antimony(III) and bismuth(III) complexes. *Eur. J. Med. Chem.* **2012**, *53*, 98–106. [[CrossRef](#)]
37. Skehan, P.; Storeng, R.; Scudiero, D.; Monks, A.; McMahon, J.; Vistica, D.; Warren, J.T.; Bokesch, H.; Kenney, S.; Boyd, M.R. New Colorimetric Cytotoxicity Assay for Anticancer-Drug Screening. *J. Natl. Cancer Inst.* **1990**, *82*, 1107–1112. [[CrossRef](#)]
38. Rigaku. *CrysAlisPro Software System*; Rigaku Oxford Diffraction: Tokyo, Japan, 2019.
39. Sheldrick, G.M. SHELXT—Integrated space-group and crystal-structure determination. *Acta Cryst.* **2015**, *A71*, 3–8. [[CrossRef](#)]
40. Dolomanov, O.V.; Bourhis, L.J.; Gildea, R.J.; Howard, J.A.K.; Puschmann, H. OLEX2: A complete structure solution, refinement and analysis program. *J. Appl. Cryst.* **2009**, *42*, 339–341. [[CrossRef](#)]
41. Bourhis, L.J.; Dolomanov, O.V.; Gildea, R.J.; Howard, J.A.K.; Puschmann, H. The anatomy of a comprehensive constrained, restrained refinement program for the modern computing environment—Olex2 dissected. *Acta Crystallogr.* **2015**, *A71*, 59–75.
42. Farrugia, L.J. WinGX and ORTEP for Windows: An update. *J. Appl. Crystallogr.* **2012**, *45*, 849–854. [[CrossRef](#)]
43. Pennington, W.T. DIAMOND—Visual crystal structure information system. *J. Appl. Cryst.* **1999**, *32*, 1028–1029. [[CrossRef](#)]